Trop J Nat Prod Res, December 2023; 7(12):5616-5622

ISSN 2616-0684 (Print)
ISSN 2616-0692 (Electronic)

Tropical Journal of Natural Product Research

Available online at https://www.tjnpr.org

Original Research Article

Morphological Changes Caused by Synthesized Zinc Oxide Nanoparticles in MDA-MB 231 Cells and Prediction with Multi-Linear Regression

Huzaifa Umar*

Operational Research Center in Healthcare, Near East University, TRNC Mersin 10, Nicosia 99138, Turkey.

ARTICLE INFO

Article history:
Received 05 October 2023
Revised 03 December 2023
Accepted 07 December 2023
Published online 01 January 2024

ABSTRACT

Developing a novel approach to treat cancerous cells while sparing healthy cells is crucial in cancer research. Plant-synthesized using Zinc Oxide Nanoparticles nanoparticles are biocompatible and stable, making them ideal for biomedical, industrial, cell imaging, and biosensor applications. This study reported the morphological development caused by synthesized Zinc Oxide Nanoparticles (ZnO-NPs-AE) in MDA-MB 231 human breast cancer cells, and a multi-linear regression (MLR) model that predicts the morphological changes was also developed. Morphological parameters such as cell body diameter (CBD), process thickness (PT) and field diameter (FD) were analyzed after treatment with various ZnO-NPs-AE concentrations and incubation for 24 hours. Significant decrease in CBD with 25, 50, 100 and 200 µg/mL ZnO-NPs-AE ($P > 0.05$; $n \geq 10$) and 2.5, 5 and 10 µg/mL of synthesized ZnO-NPs-AE did not show any significant effect on the CBD ($P < 0.05$; $n \geq 10$). Similarly, a significant decrease in PT and FD was observed with increased concentration. Furthermore, the concentration of the nanoparticles and our morphometric results were considered in MLR modelling and performance efficiency was evaluated based on correlation coefficient (R), coefficient of determination (DC), mean square error (MSE) and root mean square error (RMSE). Overall, our performance efficiency results revealed the model's ability to predict morphological changes in MDA-MB 231 cells following treatment with synthesized ZnO-NPs-AE.

Keywords: Cell body diameter; Process thickness; Nanoparticles; Correlation coefficient; Coefficient of determination.

Introduction

Developing a novel approach to treat Breast cancer (BCa) while sparing healthy cells is paramount in cancer research. The promising approach for cancer therapy nowadays is metal oxide-based chemotherapeutics. BCa is a prevalent type of malignancy that affects people worldwide, and It is a complex disease classified into five distinct developmental stages.[1,2] BCa treatment has been the subject of numerous research in recent times, with chemotherapy being the most used method.[3] However, this approach lacks the non-selectivity of medicines, leading to the loss of a high percentage of healthy and cancerous cells.[4] Due to its complications, there is a growing need for advancements in BCa detection, diagnosis, and treatment. Several studies exploring the use of natural products in preventing and treating cancer are now in place, recognizing their potential in drug discovery.[4,5] Changes in cellular morphology can serve as one of the most distinctive features of pathophysiological conditions that might promote tumour suppression and induce cell transformation.[6] Although the precise biological mechanisms underlying morphological changes during cellular metastasis have not been reported, which is known to be involved in the interaction between cells and the extracellular matrix.[7]

*Corresponding author. E mail: Huzaifa.umar@neu.edu.tr
Tel: +2348069339616

Citation: Umar H. Morphological Changes Caused by Synthesized Zinc Oxide Nanoparticles in MDA-MB 231 Cells and Prediction with Multi-Linear Regression. Trop J Nat Prod Res. 2023; 7(12):5616-5622. http://www.doi.org/10.26538/tjnpr/v7i12.36

Official Journal of Natural Product Research Group, Faculty of Pharmacy, University of Benin, Benin City, Nigeria.

Nanotechnology is an emerging field in biotechnology and medicine with promising applications such as diagnostics, targeted drug delivery, sensors, cosmetics, and imaging.[8,9] Metal and metal oxide nanoparticles have gained much attention due to their unique physicochemical properties.[10] Studies have demonstrated that synthesized zinc oxide nanoparticles (NPs) have cytotoxic potential on cancerous and normal cells, including human lens and lung epithelial cells.[11] Various synthesized zinc oxide NPs from plant sources, including *Albizia lebbeck*, *Costus pictus*, *Vitex negundo* and *Cassia auriculata*, have been reported to exhibit antiproliferative, cytotoxic and metastatic potentials on various cell lines.[12-15] Due to the potential of metal oxide NPs in cancer research, we explore a multi-linear regression (MLR) model while considering some variables to predict the impact of these NPs in cancer treatment.

Modelling in vitro data has been a venerable challenge due to molecular and cellular regulatory mechanisms' complexities.[16] Machine Learning (ML) algorithms use various training data to make a useful prediction that can be used to enhance research activities and provide promising solutions.[17] Assisting pathologists with algorithms effectively improves the efficiency and sensitivity in detecting micrometastasis.[18] Fang et al. use MLR to develop a model to identify potential enzyme inhibitors for choosing compounds during molecular synthesis for effective drug discovery.[19-21] MLR analysis was used in the evaluation of nitrate sources as a result of bacterial denitrification to determine the parameters with the highest impact on output uncertainty.[19, 21] However, due to the wide application and efficiency of MLR in prediction, we utilized the model in the prediction of morphological changes caused by synthesized NPs from in vitro experimental analysis results, and it differs from other models as it utilized our experimental data to predict morphological changes with precision, predictability and interpretability.

In this present study, morphological development caused by synthesized Zinc Oxide Nanoparticles (ZnO-NPs-AE) in MDA-MB

231 human BCa cells was observed. Furthermore, the MLR model that predicts the morphological changes was also developed from our experimental data to find the best relationship between the concentration of our NPs and morphological parameters.

Methods

Plant Collection and Identification

Fresh flowers of *Mentha piperita (M P)* were collected from a farm in Lefkosa (Lat.34° and 36° **N**; Long 32° and 35° **E**) in November 2021, Turkish Republic of Northern Cyprus and authenticated by Prof. Dr. Ibrahim Baktir at the Botany Department of Cyprus International University, and a voucher number of CIU/BOT/0012 was given to the specimen, and deposited at the herbarium of the department for reference. Triple distilled deionized water was used to prepare all the aqueous solutions of the plant material.

All the chemicals and reagents utilized throughout the experiment are of analytical grade. The chemicals used include zinc nitrate ($Zn(NO_3)_2{\cdot}6H_2O$) solutions, Dimethyl Sulfoxide (DMSO) (Sigma-Aldarich Inc.), Dulbecco's Modified Eagle Medium (DMEM) (Gibco by Life Technologie, USA), Fetal Bovine Serum (FBS) (Gibco by Life Technologies, USA), Glycine (Sigma-Aldarich Inc.), 0.25% Trypsin and 0.4 % Tryphan Blue (Gibco by Life Technologies, USA), L-Glutamine 200 mm (Gibco by Life Technologies, USA), Distilled Water (Gibco by Life Technologies, USA), 70% Ethanol (Merck), Penicillin (Gibco by Life Technologies, USA).

Biosynthesis of Zinc Oxide Nanoparticles and Characterization

The synthesis of ZnO-NPs-AE using *Mentha piperita* was conducted following the method used by Umar et al. with slight modifications.[22] Zinc nitrate ($Zn(NO_3)_2{\cdot}6H2O$) (0.05 M solution) was used for the synthesis of the NPs. The extraction process involved using water as the solvent in a conical flask and was carried out for 72 hours at 45°C. During the procedure, a 15% aqueous extract of *Mentha piperita* was gradually added under constant stirring at 70°C for a period of 9 hours. The pH level was adjusted using NaOH solution during the shaking process. Finally, the mixture was calcined in a muffle furnace. The resulting residue is the synthesized ZnO-NPs-AE.

The characterization of the synthesized NPs was reported in our previous studies,[21] in which UV-Vis spectroscopy was conducted using a Shimadzu UV-2450 instrument, in which the NPs were dissolved in deionized water and thoroughly mixed with a sonicator and colour shift was observed as shown in Figure 1. The resulting solution was then filtered and placed in a 10 mm cuvette, where the spectrum was measured across the wavelength range of 200 to 900 nm at room temperature (Figure 2a). Furthermore, we identified the functional groups in the ZnO-NPs-AE by employing a Fourier Transform Infrared Spectrophotometer (FTIR) operating at a 500-4000^{cm-1} frequency range (Figure 2b). The crystalline nature of the NPs was assessed using the Rigaku ZSX Primus II X-ray diffractometer (XRD) (Figure 2c). This involved using powdered samples in the X-ray diffractometer, equipped with CuK radiation, to examine the structural characteristics of the NPs. Additionally, the morphological structure of the nanoparticles was examined using a scanning electron microscope (SEM), and we conducted elemental mapping through energy-dispersive X-ray spectroscopy (EDX) (Figure 2d and e).

The synthesized nanoparticles were characterized using various spectroscopic and microscopic analyses; FTIR analysis was carried out to identify the distribution of the attached functional group on the surface of the NPs. Water was absorbed during the synthesis, resulting in the O-H bond at absorption bands of 3420 $^{cm-1}$. Additionally, C=CH of a methyl group and C=O of alcohol (saturated) were observed at 1049 $^{cm-1}$ and 1450 $^{cm-1}$, respectively. The X-ray diffraction peaks obtained from the synthesized NPs confirmed their spherical phase, crystal formation, and purity, as seen in Figure 2c. The Debye-Scherrer formula was employed to calculate the diameter of the NP crystallites, which were found to be 23 nm based on the diffraction peaks observed at 76.58°, 72.53°, 67.66°, 62.78°, 56.48°, 47.54°, 34.34° and 31.70° SEM analysis further confirmed that the synthesized NPs are spherical in shape with an average size of 23nm, as depicted in Figure 1d. Additionally, the EDS analysis revealed that the synthesized NPs are indeed zinc oxide NPs, with signals indicating the presence of zinc and oxygen, as shown in Figure 1e.

Cell lines and Culture Conditions

As part of our study, MDA-MB 231 cell line obtained from Imperial College London (UK), which is renowned for its metastatic capabilities, was used. These cells were safely stored at the Biotechnology Research Centre (BCR) of Cyprus International University and were approved for use by the BCR ethical committee (BRCEC2011-01). We utilized DMEM supplemented with 2 mM L-glutamine, penicillin, and 10% fetal bovine serum (FBS) to culture the cells. The cells were maintained in a sterile incubator at a temperature of 37°C and 5% CO_2.

Treatment, Fixation and Staining

MDA-MB 231 cells plated in 35 mm tissue culture dishes ($3x10^4$ cells/dish) were treated with various concentrations of the synthesized ZnO-NPs-AE and allowed to settle overnight. Then, various concentrations (0 ~ 200 µg/mL) of the synthesized ZnO-NPs-AE were added to cells and incubated for 24 hours. After the treatment, the cells were washed several times immediately with a 0.1 M phosphate-buffered saline solution (PBS) at 37°C. Then, they were fixed (a process called fixation) for 20 minutes at 4°C with 8% freshly prepared paraformaldehyde. The cells were rewashed with PBS and stained with crystal violet dye.

Morphometric Analysis

Possible effects of ZnO-NPs-AE on some cellular morphological parameters were studied using the method of Fraser et al. with some modificarions.[23] Cellular parameters studied illustrated in Fig. 3, the field diameter (FD) defined as the distance between extreme ends of the cell, cell body diameter (CBD) defined as the closest circle diameter that fits into the body of the cell and process thickness (PT) defined as thickness of the half of the length of the cell were analyzed. Cells (3×10^4/mL) in 35 mm dishes were plated and allowed to settle. The cells were then treated with different concentrations (0 ~ 200 µg/mL) of ZnO-NPs-AE for 24 hours. After the treatment, cells were randomly selected and viewed using a digital camera (Leica DF295, German) mounted on the inverted microscope at x20 magnification. ImageJ software was employed to quantitatively analyze chosen images.

Modelling Approach

The approach used in this analysis was based on our experimental data. The concentration of the synthesized ZnO-NPs-AE and morphological parameters such as cell body diameter (CBD), process thickness (PT) and field diameter (FD) of MDA-MB were considered in modelling, even though other parameters can be considered for the same purpose. Furthermore, MLR was considered for the prediction of various parameters.[24] The independent and dependent variables in path models are represented as boxes or rectangles. The exogenous area contains single-headed arrows exiting from them; a double-headed arrow indicates that variables are solely correlated.

Overview of Multi Linear Regression

The use of Multiple Linear Regression (MLR) is a sophisticated statistical method that involves multiple independent variables to explain the behavior of a dependent variable. Linear regression is a statistical technique used to describe and model the relationship that exists between a dependent variable and one or more independent variables and is achieved by fitting linear equations to a set of data. The best-fit line is determined by reducing the sum of the squares of the vertical deviations between the line and the observed data. A good MLR model should explain the dependent variable with fewer independent variables.[25]

The choice between simple linear regression (SLR) and multiple linear regression (MLR) depends on the target objectives of the prediction. In SLR, a single predictor is compared to a single variable. Additionally, MLR analyses the relationship between one dependent variable and more than one independent variable.[26] MLR-based

ISSN 2616-0684 (Print)
ISSN 2616-0692 (Electronic)

models that predict morphological changes in cells treated with ZnO-NPs-AE were build using MLR option in statistics tool box in MATLAB (R2017a) was used to build the that predict morphological. The technique of Multiple Linear Regression (MLR) can be expressed mathematically using the following equation (1):

$$y = a_0 + a_1x_1 + a_2x_2 + \cdots a_ix_i \quad (1)$$

Where x_1 denotes predictor, a_0 regression constant, a_i the coefficient of the i and N is number data set ($n \geq 10$).

Model Performance Criteria

In this study, different statistical error measures were used to model our experimental morphological result based on equations (2) to (5). The goodness-of-fit measure used was the determination coefficient (DC). Other measures included the mean squared error (MSE), root mean squared error (RMSE) and the correlation coefficient (R).

$$R = \frac{\sum_{i=1}^{N} (Y_{obs}-\bar{Y}_{obs})(Y_{com}-\bar{Y}_{com})}{\sqrt{\sum_{i=1}^{N} (Y_{obs}-\bar{Y}_{obs})^2 \sum_{i=1}^{N} (Y_{com}-\bar{Y}_{com})^2}} \quad (2)$$

$$\text{DC} = 1 - \frac{\sum_{j=1}^{N}[(Y)_{obs,j}-(Y)_{com,j}]^2}{\sum_{j=1}^{N}[(Y)_{obs,j}-\overline{(Y)}_{obs,j}]^2} \quad (3)$$

$$RMSE = \sqrt{\frac{1}{N}\sum_{j=1}^{N}\left((Y)_{obs,j} - (Y)_{com,j}\right)^2} \quad (4)$$

$$\text{MSE} = \frac{1}{N}\sum_{i=1}^{N} (Y_{obsi} - Y_{comi})^2 \quad (5)$$

Results and Discussion

The biosynthesis of ZnO-NPs-AE using *Mentha piperita* as a stabilizing agent was confirmed by observing a colour shift as shown in Figure 1 and conducting a characterization analysis. Its effect on some of the morphological parameters, such as cell body diameter (CBD), process thickness (PT) and field diameter (FD) of MDA-MB 231 cancer cells, was studied (Figure 3). Treatment of MDA-MB 231 for 24 h with 2.5, 5 and 10 µg/mL of NP did not show any effect on the CBD ($P > 0.05$; $n \geq 10$; Figure 4a), but higher concentrations (200, 100, 50, and 25 µg/mL) showed decreased in CBD significantly when compared with the control group ($P < 0.05$; $n \geq 10$; Figure 4a). The effects of ZnO-NPs-AE on CBD of MDA-MB 231 cells after 24 h incubation was found to be concentration dependent. Likewise, a significant decrease in PT was observed with increased concentration ($P < 0.05$; $n \geq 10$; Figure 4b). Similarly, treatment with ZnO-NPs-AE following the 24-hour incubation period revealed a significant decrease in FD ($P > 0.05$; $n \geq 10$; Figure 4c). A multiple comparison table between various concentrations of the ZnO-NPs-AE and control was shown in Table 1.

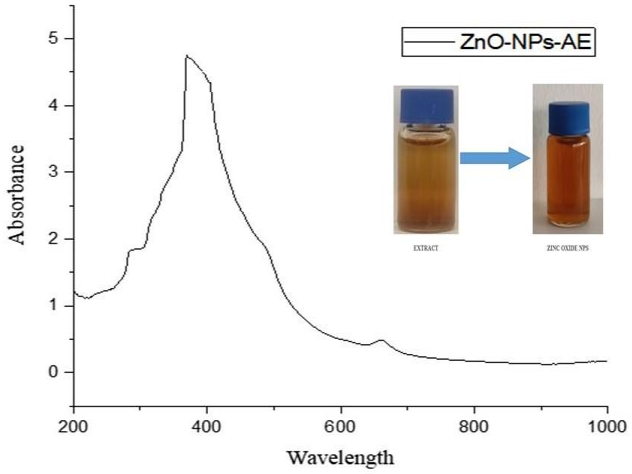

Figure 1: UV-vis spectrum of biosynthesized zinc oxide nanoparticles (ZnO-NPs-AE) using *Mentha piperita* extract.

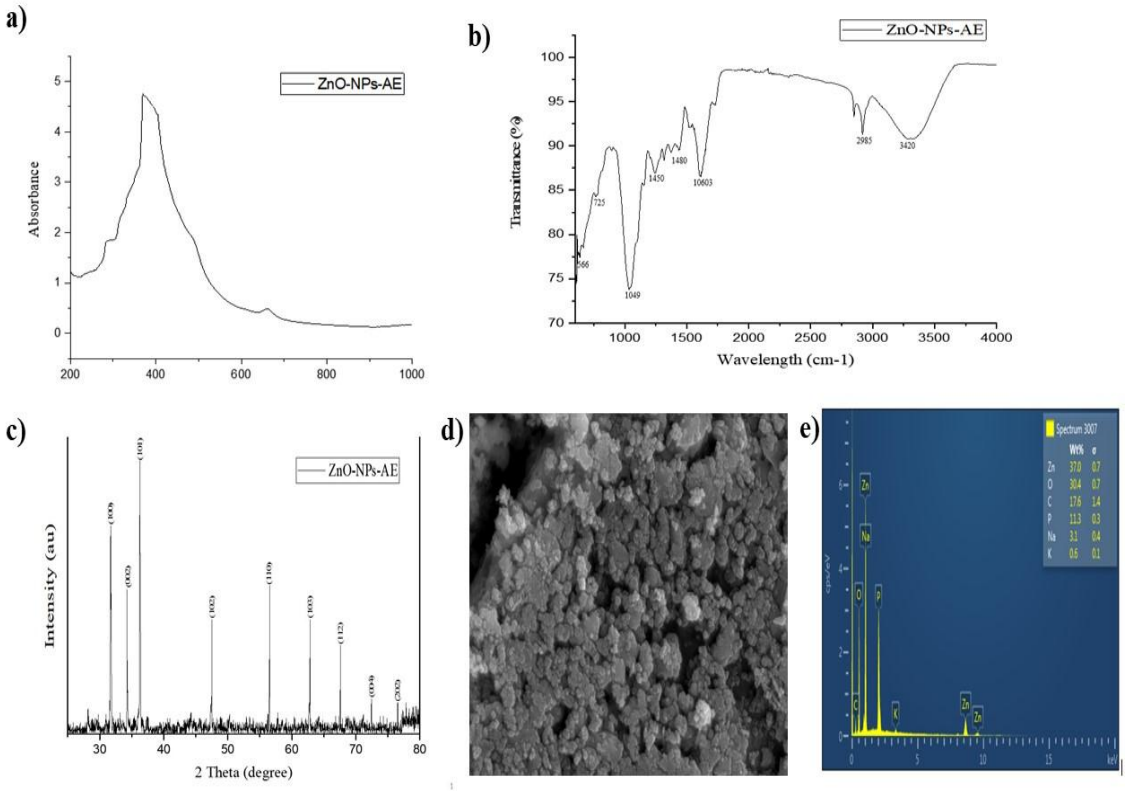

Figure 2. (a) UV-vis spectra (b) FTIR of (c) XRD pattern (d) SEM image and (e) EDS of zinc oxide nanoparticles (ZnO-NPs-AE) synthesized using *Mentha piperita* aqueous extract. Adapted from Umar *et al.*[22]

ISSN 2616-0684 (Print)
ISSN 2616-0692 (Electronic)

Table 1: Multiple Comparison table between the various concentrations of synthesized ZnO-NPs-AE and Morphological parameters

ZnO-NPs-AE Concentration (µg/mL)			CBD	PT	FD	ZnO-NPs-AE Concentration (µg/mL)			CBD	PT	FD
P < 0.05											
Control	vs	2.5	-	*	*	5.0	vs	100	-	***	***
Control	vs	5.0	-	*	***	5.0	vs	150	***	***	***
Control	vs	10.0	-	**	***	5.0	vs	200.0	***	***	***
Control	vs	25.0	***	***	***	10.0	vs	25.0	**	***	***
Control	vs	50. 0	***	***	***	10.0	vs	50. 0	***	***	***
Control	vs	100	***	***	***	10.0	vs	100.0	***	*	***
Control	vs	150	***	***	***	10.0	vs	150.0	*	**	***
Control	vs	200	***	***	***	10.0	vs	200.0	***	***	***
2.5 µg/mL	vs	5.0	-	*	*	25.0	vs	50. 0	**	***	***
2.5 µg/mL	vs	10.0	-	**	**	25.0	vs	100.0	***	**	***
2.5 µg/mL	vs	25.0	***	***	***	25.0	vs	150.0	***	***	**
2.5 µg/mL	vs	50	***	***	***	25.0	vs	200.0	***	***	***
2.5 µg/mL	vs	100	***	***	***	50. 0	vs	100.0	***	***	***
2.5 µg/mL	vs	150	***	***	***	50. 0	vs	150.0	**	***	***
2.5 µg/mL	vs	200	***	***	***	50. 0	vs	200.0	***	**	***
5.0 µg/mL	vs	10.0	-	-	**	100.0	vs	150.0	-	**	*
5.0 µg/mL	vs	25.0	*	**	***	100.0	Vs	200.0	**	***	***
5.0 µg/mL	vs	50. 0	***	***	***	150.0	Vs	200.0	-	**	***

analysed using one-way ANOVA followed by Newman-Keuls *post hoc* analysis. (*) P < 0.05; (**) P < 0.01 and (***) P < 0.0001.

Table 2: Result of MLR models

	Training				Testing			
	R	**DC**	**RMSE**	**MSE**	**R**	**DC**	**RMSE**	**MSE**
MLR-FD-MDA-MB 231	0.985	0.989	0.062	0.004	0.968	0.971	0.041	0.002
MLR-CBD-MDA-MB 231	0.989	0.993	0.056	0.003	0.958	0.969	0.037	0.001
MLR-PT-MDA-MB 231	0.991	0.994	0.058	0.003	0.971	0.973	0.043	0.001

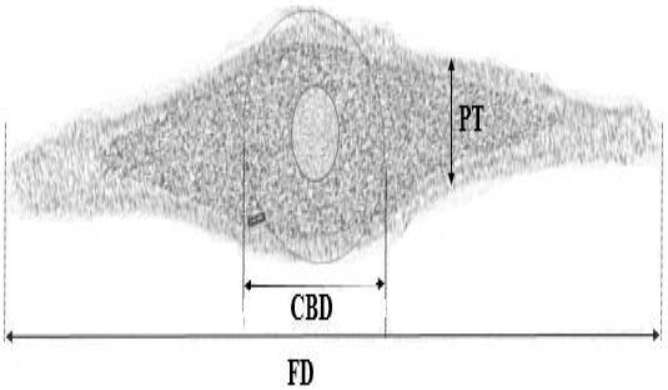

Figure 3: Bipolar cell schematic diagram illustrating parameters measured as quantitative determinants of cellular morphology. Field diameter (FD) defined as the distance between extreme ends of the cell. Cell body diameter (CBD) defined as diameter of the closest circle that fit into cell body. Process thickness (PT) defined as thickness of the half of the length of the cell.

The result obtained in our studies showed morphological changes caused as a result of treatment with various concentrations of the ZnO-NPs-AE and agrees with the result revealed by Fraser et al.[21] Enhancing the metastatic potential of MAT-LyLu rat prostate cancer cells by manipulating their morphological development when treated with tetrodotoxin.[21] Alternatively, Na^+ channel activity can be influenced by changes in cellular morphology as a result of alterations of intracellular Ca^{2+} levels or exchange Ca^{2+}- Na^+ .[27,28] Synthesized ZnO NPs induced cell death, and the cell death might be a result of morphological changes induced through the mitochondria signalling pathway.[29]

Our experimental result showed a linear relationship between the concentration of the synthesized NPs, CBD, PT and FD, and significant differences in the variables were observed. Linear classical MLR was used to predict the morphological changes observed following treatment with our synthesized NPs using our experimental data. Performance indices of the models, such as correlation coefficient (R), coefficient of determination (DC), mean square error (MSE), and root mean square error (RMSE), were determined using MATLAB 9.3 (R2017a). The MLR model showed good performance in revealing the correlation between various concentrations of the synthesized NPs and the morphological parameters used in the prediction, as shown in Table 2. Furthermore, the modelling performance of our MLR using R, DC, MSE, and RMSE confirmed the strong ability of MLR to predict treated cell morphological

ISSN 2616-0684 (Print)
ISSN 2616-0692 (Electronic)

changes with minimal standard error. Figure 5 shows the RMSE and MSE of the morphometric prediction of MDA-MB 231 cells in both testing stages, and good performance was observed in both stages. Variation in R and DC demonstrated in our surface rate chart (Figure 6) revealed the excellent performance of our model, and various studies revealed that variation in R and DC of any model is attributed to the model's good performance.[30] In addition, the spread of the data was assessed using Surface response simulation (Figure 7), and the response of the measured values and the data spread were evaluated.

Conclusion

Stable Zinc oxide nanoparticles synthesized using *Mentha piperita* as a chelating agent, characterized in our previous studies, revealed morphological changes in MDA-MB 231 cells in a concentration-dependent manner. Morphological parameters such as cell body diameter (CBD), process thickness (PT) and field diameter (FD) were analyzed following treatment with various concentrations. Furthermore, a multi-linear regression (MLR) model was used to predict the morphological development caused following treatment with ZnO-NPs-AE. Performance indices of the MLS model, such as correlation coefficient (R), coefficient of determination (DC), mean square error (MSE) and root mean square error (RMSE), were considered in determining the efficiency of the model. Overall, our performance efficiency results revealed the model's ability to predict morphological changes in MDA-MB 231 cells following treatment with synthesized ZnO-NPs-AE. Artificial neural networks and other models should be employed to predict morphological changes in cancer cells.

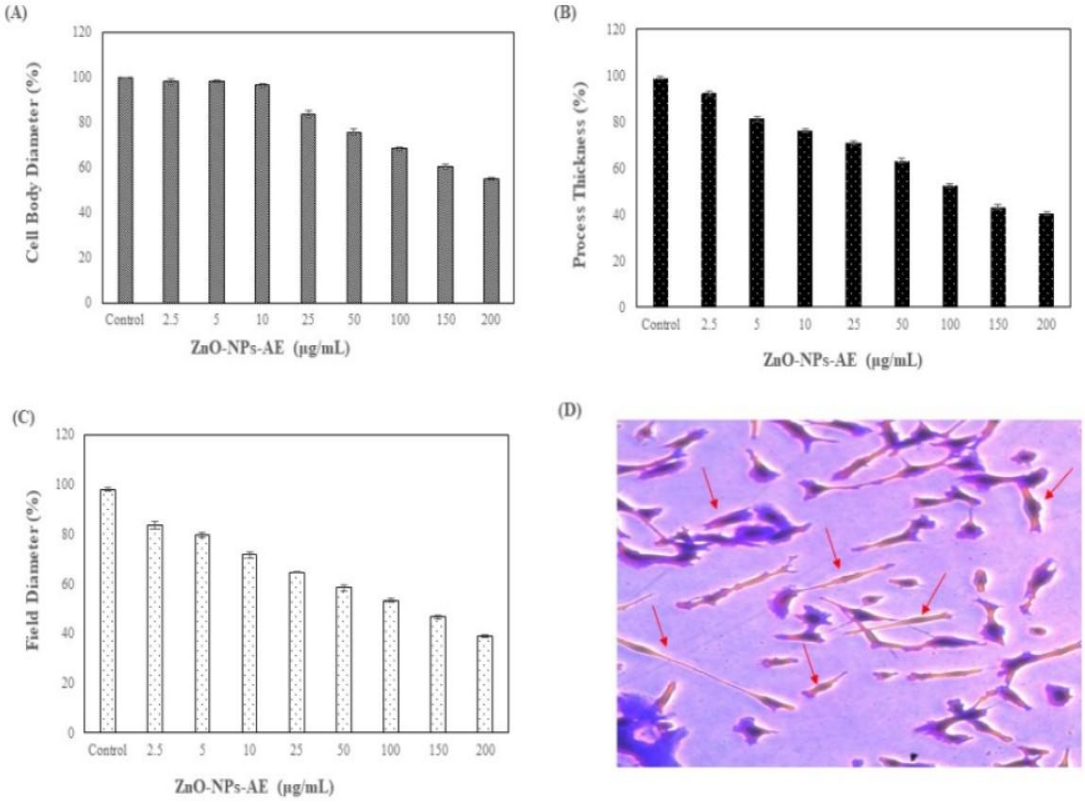

Figure 4: Effect of synthesized ZnO-NPs-AE on (a) cell body diameter (CBD), (b) Process Thickness (PT), (c) Field Diameter (FD), and (D) Phase contrast photomicrographs (20x), of MDA-MB 231 cells treated with synthesized NPs

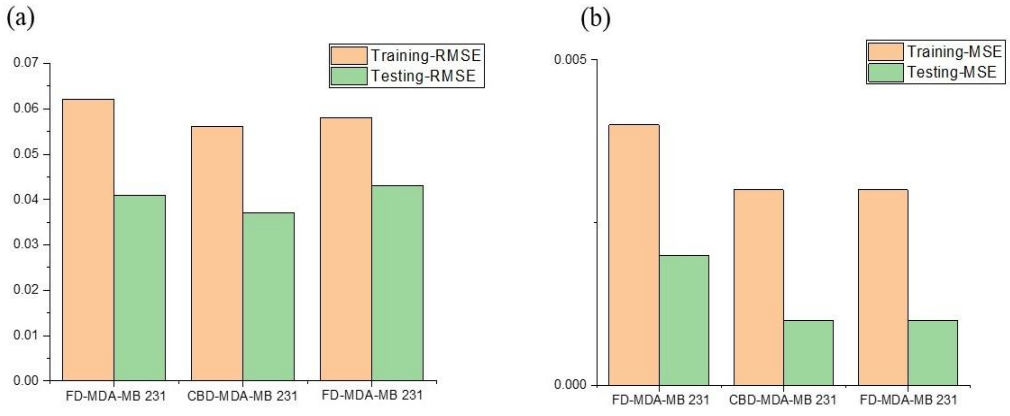

Figure 5: Morphometric prediction of treated MDA-MB 231 using synthesized ZnO-NPs-AE in both training and testing stages. (a) Relative mean square error (RMSA) and (b) mean square error (MSE).

ISSN 2616-0684 (Print)
ISSN 2616-0692 (Electronic)

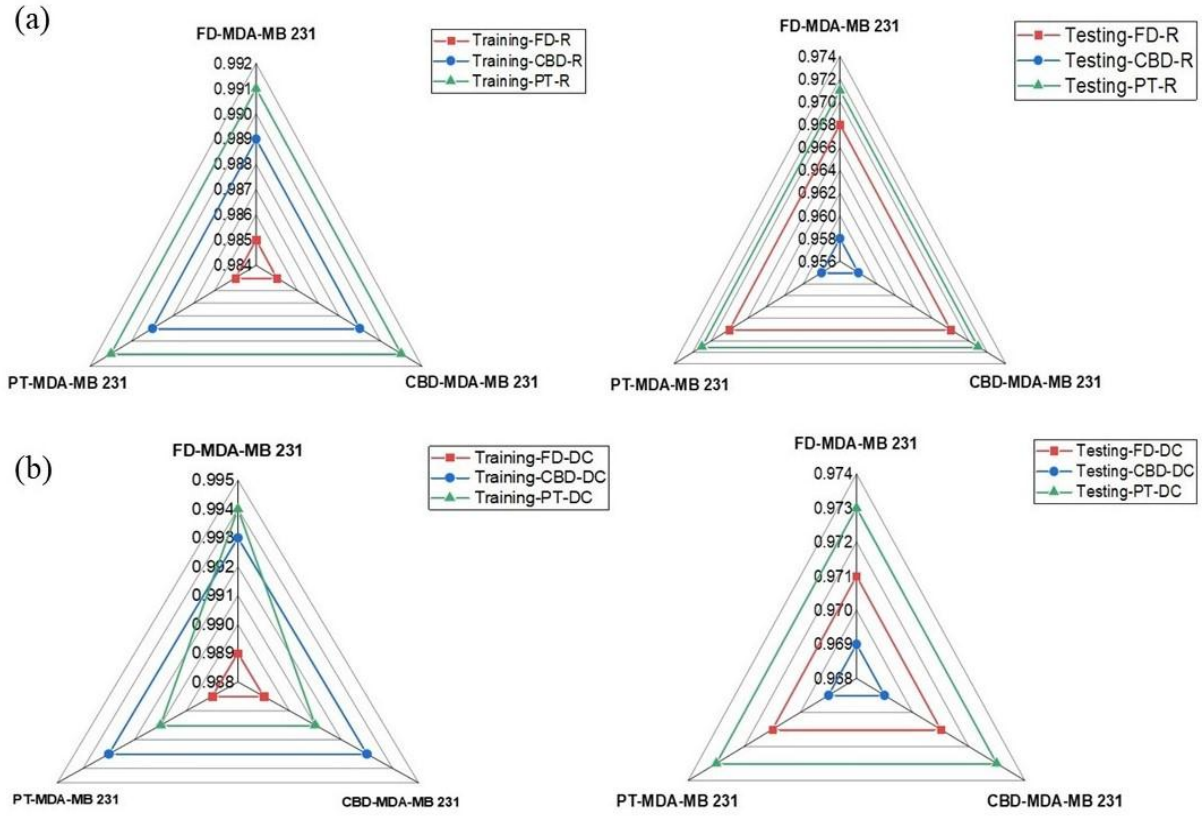

Figure 6: Radar chart for (a) Correlation coefficient (R), and (b) determination coefficients.

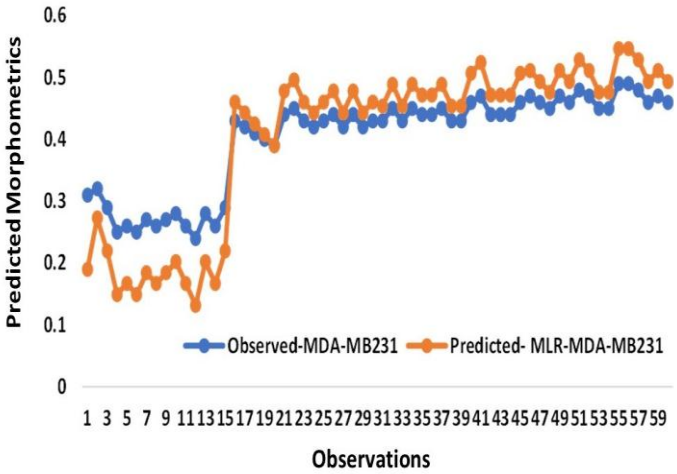

Figure 7. Response surface simulation for morphological changes observed in MDA-MB 231 treated with synthesized ZnO-NPs-AE.

Conflict of Interest

The authors declare no conflict of interest.

Authors' Declaration

The authors hereby declare that the work presented in this article is original and that any liability for claims relating to the content of this article will be borne by them.\

References

1. McGuire S. World Cancer Report 2014. Geneva, Switzerland: World Health Organization, International Agency for Research on Cancer, WHO Press, 2015. Adv Nutr. 2016; 15;7(2):418-9. https://doi.org/10.3945/an.116.012211.
2. Lebeau A, and Denkert C. Updated WHO classification of tumors of the breast: the most important changes. Pathologe. 2021; 2(3):270-280. https://doi.org/10.1007/s00292-021-00934-9.
3. Ubhenin AE, Ikebuiro JO, Idris RI, Anura F, Erharuyi O. Exploring Mechanisms of Tumorigenesis and Plant-Based Therapies: A Comprehensive Review of Cancer Pathogenesis and Treatment Strategies. Trop J Nat Prod Res. 2023; 7(11):5026-5033. http://www.doi.org/10.26538/tjnpr/v7i11.2.
4. Kooti W, Servatyari K, Behzadifar M, Asadi-Samani M, Sadeghi F, Nouri B, Zare Marzouni H. Effective Medicinal Plant in Cancer Treatment, Part 2: Review Study. J Evid Based Complementary Altern Med. 2017; (4):982-995. https://doi.org/10.1177/2156587217696927.
5. Shareef M, Ashraf MA, Sarfraz M. Natural cures for breast cancer treatment. Saudi Pharm J. 2016; 24(3):233-40. https://doi.org/10.1016/j.jsps.2016.04.018.
6. Sastrodihardjo S, Sasaki Y, Shiba Y, Kanno Y. Possible involvement of reorganization of actin filaments, induced by tumor-promoting phorbol esters, in changes in colony shape and enhancement of proliferation of cultured epithelial cells. J Cell Physiol. 1987; 132(1):49-56. https://doi.org/10.1002/jcp.1041320107.
7. Mohler JL, Bakewell WE, Sharief Y, Coleman WB, Chay CH, Silvers SM, Smith GJ. Detection of candidates for cancer cell motility inhibitory protein in the Dunning adenocarcinoma model. Clin Exp Metastasis. 1995; 13(6):474-80. https://doi.org/10.1007/BF00118186.

8. Kavaz D, Umar H, Aliyu MR. Green Synthesized Metallic Oxide Nanomaterials for Diverse Applications. J Nanoworld. 2022; 8(1):14-22. https://doi.org/10.17756/nwj.2022-096.
9. Halilu EM, Ngweh VA, Airemwen CO. Green Synthesis of Silver Nanoparticles from *Parinari curatellifolia* Methanol Stem Bark Extract and Evaluation of Antioxidant and Antimicrobial Activities. Trop J Nat Prod Res. 2023; 7(3):2498-2505 http://www.doi.org/10.26538/tjnpr/v7i3.5.
10. Kavaz D, Umar H, Shehu S. Synthesis, characterization, antimicrobial and antimetastatic activity of silver nanoparticles synthesized from *Ficus ingens* leaf, Artificial Cells, Nanomedicine and Biotechnology. 2018; 46(sup3). https://doi.org/10.1080/21691401.2018.1536060
11. Wang B, Zhang J, Chen C, Xu G, Qin X, Hong Y, Bose DD, Qiu F, Zou Z. The size of zinc oxide nanoparticles controls its toxicity through impairing autophagic flux in A549 lung epithelial cells. Toxicol Lett. 2018; 15;285:51-59. https://doi.org/10.1016/j.toxlet.2017.12.025.
12. Sundrarajan M, Ambika S, and Bharathi K. Plant-extract mediated synthesis of ZnO nanoparticles using *Pongamia pinnata* and their activity against pathogenic bacteria. Adv. Powder Tech. 2015; 26(5). https://doi.org/10.1016/j.apt.2015.07.001.
13. Padalia H, Moteriya P. Chanda S. Synergistic Antimicrobial and Cytotoxic Potential of Zinc Oxide Nanoparticles Synthesized Using *Cassia auriculata* Leaf Extract", BioNanoScience, 2018; 8(1). https://doi.org/10.1007/s12668-017-0463-6.
14. Suresh J, Ganeshan P, Vincent A, Mahalingam S, Sun I H. Green synthesis and characterization of zinc oxide nanoparticle using insulin plant (*Costus pictus D. Don)* and investigation of its antimicrobial as well as anticancer activities. Advances in Natural Sciences: Nanoscience and Nanotechnology. 2018; 9(1). https://doi.org/10.1088/2043-6254/aaa6f1.
15. Umar H, Kavaz D, Rizaner N. Biosynthesis of zinc oxide nanoparticles using *Albizia lebbeck* stem bark, and evaluation of its antimicrobial, antioxidant, and cytotoxic activities on human breast cancer cell lines. Int J Nanomedicine. 2018; 20;14:87-100. https://doi.org/10.2147/IJN.S186888.
16. Kusumoto D, Yuasa S. The application of convolutional neural network to stem cell biology. Inflamm Regener. 2019; 39, 14. https://doi.org/10.1186/s41232-019-0103-3.
17. Sivaramakrishnan N, Subramaniyaswamy V, and Indragandhi V. Multi-Linear Regression Technique for Predicting the Liver Disease. Innov. in Power and Adv. Computing Tech. (i-PACT). 2021. pp. 1-7. https://doi.org/10.1109/i-PACT52855.2021.9696792.
18. Steiner, D. F. *et al.* (2018) "Impact of Deep Learning Assistance on the Histopathologic Review of Lymph Nodes for Metastatic Breast Cancer", American J Surgical Pathol. 2021; 42(12). https://doi.org/10.1097/PAS.0000000000001151.
19. Zheng F, Zhan M, Huang X, Abdul Hameed MD, Zhan CG. Modeling in vitro inhibition of butyrylcholinesterase using molecular docking, multi-linear regression and artificial neural network approaches. Bioorg Med Chem. 2014; 1;22(1):538-49. https://doi.org/10.1016/j.bmc.2013.10.053.
20. Hadi S, Setiawan D, Viogenta P, SunardiS, Nastiti K, Nisa K, Andiarsa D.Molecular Docking and Dynamics Study of Compounds from Combretum indicumvar. B Seeds as Alcohol Dehydrogenase Inhibitors. Trop J Nat Prod Res. 2023; 7(11):5087-5096.http://www.doi.org/10.26538/tjnpr/v7i11.11.
21. Meghdadi A, and Javar N. Evaluation of nitrate sources and the percent contribution of bacterial denitrification in hyporheic zone using isotope fractionation technique and multi-linear regression analysis. J Environ. Manag. 2018; 222: 54-65. https://doi.org/10.1016/j.jenvman.2018.05.022.
22. Huzaifa U, Abdullahi GU, Maryam. RA, Dilber UO. (2023) "Phytofabrication of Zinc Oxide Nanoparticles Using Cyprus *Mentha Piperita* and Evaluation of its Anticancer And Antimicrobial Activity. European Chemical Bulletin. 2023; 12(6),7632–7638. htttps://doi.org/10.48047/ecb/2023.12.si6.678.
23. Fraser SP, Ding Y, Liu A, Foster CS, Djamgoz MB. Tetrodotoxin suppresses morphological enhancement of the metastatic MAT-LyLu rat prostate cancer cell line. Cell Tissue Res. 1999; 295(3):505-12. doi: 10.1007/s004410051256. PMID: 10022970.
24. Ghali UM, Usman AG, Chellube ZM, *et al*. Advanced chromatographic technique for performance simulation of anti-Alzheimer agent: an ensemble machine learning approach. SN Appl. Sci. 2020; **2**, 1871. https://doi.org/10.1007/s42452-020-03690-2.
25. Sinharay S. An Overview of Statistics in Education. Editor(s): Penelope Peterson, Eva Baker, Barry McGaw. International Encyclopedia of Education (Third Edition). Elsevier. 2010; 1-11. ISBN 9780080448947. https://doi.org/10.1016/B978-0-08-044894-7.01719-X.
26. Umar H, Rizaner N, Usman AG, Aliyu MR, Adun H, Ghali UM, Uzun Ozsahin D, Abba SI. Prediction of Cell Migration in MDA-MB 231 and MCF-7 Human Breast Cancer Cells Treated with *Albizia Lebbeck* Methanolic Extract Using Multilinear Regression and Artificial Intelligence-Based Models. Pharmaceuticals (Basel). 2023; 8;16(6):858. https://doi.org/10.3390/ph16060858.
27. Klarsfeld A, Laufer R, Fontaine B, Devillers Thiéry A, Dubreuil C, Changeux JP. Regulation of muscle AChR α subunit gene expression by electrical activity: Involvement of protein kinase C and Ca 2^{+}. Neuron. 1989; 2(3). https://doi.org/10.1016/0896-6273(89)90307-3.
28. Hahn CG, Covault J. Neural regulation of N-cadherin gene expression in developing and adult skeletal muscle. Journal of Neuroscience. 1992; 12(12). https://doi.org/10.1523/jneurosci.12-12-04677.1992.
29. Ling W, Chao C, Lijie G, Qin L, Hongyan D, Hongsheng B, Dadong G. Zinc oxide nanoparticles induce murine photoreceptor cell death via mitochondria-related signaling pathway, Artificial Cells, Nanomedicine, and Biotechnology. 2018; 46:sup1, 1102-1113. https://doi.org/10.1080/21691401.2018.1446018.
30. Adun H, Doga K, Mustafa D, Huzaifa U, Ifeoluwa W. An experimental investigation of thermal conductivity and dynamic viscosity of Al2O3-ZnO-Fe3O4 ternary hybrid nanofluid and development of machine learning model. Powder Technology, 2021; 394. https://doi.org/10.1016/j.powtec.2021.09.039.